frontiers | Frontiers in Materials

TYPE Original Research
PUBLISHED 08 August 2024
DOI 10.3389/fmats.2024.1391066

OPEN ACCESS

EDITED BY
Adebowale Martins Obalalu,
Augustine University Ilara Epe, Nigeria

REVIEWED BY
MD. Shamshuddin,
SR University, India
Asad Ullah,
University of Lakki Marwat, Pakistan

*CORRESPONDENCE
Umair Khan,
umair.khan@lau.edu.lb

RECEIVED 24 February 2024
ACCEPTED 23 July 2024
PUBLISHED 08 August 2024

CITATION
Elattar S, Khan U, Zaib A, Ishak A, Alwadai N and Albalawi H (2024), Irreversible mechanism and thermal cross-radiative flow in nanofluids driven along a stretching/shrinking sheet with the existence of possible turning/critical points.
Front. Mater. 11:1391066.
doi: 10.3389/fmats.2024.1391066

Irreversible mechanism and thermal cross-radiative flow in nanofluids driven along a stretching/shrinking sheet with the existence of possible turning/critical points

Samia Elattar[1], Umair Khan[2,3,4,5]*, Aurang Zaib[6], Anuar Ishak[2], Norah Alwadai[7] and Hind Albalawi[7]

[1]Department of Industrial and Systems Engineering, College of Engineering, Princess Nourah bint Abdulrahman University, Riyadh, Saudi Arabia, [2]Department of Mathematical Sciences, Faculty of Science and Technology, Universiti Kebangsaan Malaysia, Bangi, Selangor, Malaysia, [3]Department of Mathematics, Faculty of Science, Sakarya University, Serdivan, Türkiye, [4]Department of Computer Science and Mathematics, Lebanese American University, Byblos, Lebanon, [5]Department of Mechanics and Mathematics, Western Caspian University, Baku, Azerbaijan, [6]Department of Mathematical Sciences, Federal Urdu University of Arts, Science and Technology, Gulshan-e-Iqbal Karachi, Pakistan, [7]Department of Physics, College of Science, Princess Nourah bint Abdulrahman University, Riyadh, Saudi Arabia

The significant increase in thermal efficiency and the rate of energy exchange used in fuel dynamics and automobile coolants are leading to a better understanding of nanofluids. This computational analysis explores the thermal conductivity performance for radiative cross-flow of a nanofluid across an expanding/constricting sheet with a suction effect as a result of its application. To compute or calculate the magnificent point of nanofluid flow, the entropy, and asymmetrical heat source/sink effects are also elicited. The boundary layers traverse a stream-wise procedure for expanding and contracting sheets. Additionally, the study examines the features of heat transfer and cross-flow of nanofluids using numerical simulations. By employing similarity variables, the basic PDE equations of the current model are transformed into ODEs, and they are subsequently evaluated using the bvp4c method. Therefore, the effects of embedded flow variables on drag force, heat transfer rate, and entropy generation profiles have been framed using parametric research. Multiple solutions are offered for a specific range of the contracting parameter as well as the mass suction parameter. In addition, the heat transfer rate accelerates due to the heat source and decelerates due to the heat sink. The literature that is already published has been compared favorably, and it reveals many commonalities.

KEYWORDS

cross flow, entropy generation, expanding/contracting sheet, irregular heat source/sink, nanofluid

1 Introduction

The nanofluid has a large number of nanoparticles and nanometer-sized molecules. Tiny particles are disseminated (added) in fluids to increase their heat transfer capabilities, even though the structure and content of nano-molecules depend on carbides, metals, and carbon nanotubes. The combinations that make up the nanofluid are typically combined with particles of average nanoscale size. Nanotubes, nanofibers, nanowires, nanoparticles, nanosheets, nanorods, and other materials are routinely made with nanofluids. The most effective and practical methods have been developed and put into practice for the modeling of nanofluid flow models, while the addition of specific materials of a particular kind has increased the thermal conductivity of various fluids. Several engineering procedures use nanoparticles in fluids to improve heat transfer. Equipment like heat exchangers in heavy machinery, automobiles, and industries is highly dependent on effective energy transfer. With these applications in mind, Choi and Eastman (Choi and Eastman, 1995) developed nanofluids to enhance the heat transfer capabilities of ordinary fluids. According to Eastman et al. (Eastman et al., 2001), adding copper nanoparticles to ethylene glycol at a concentration of 0.3 volumes results in a 40% increase in thermal conductivity. Khan and Pop (Khan and Pop, 2010) have numerically addressed the issue of laminar fluid flow that develops when a flat surface is stretched in a nanofluid. It was discovered that the reduced heat transfer is a diminishing function of every single dimensionless number. The numerical solution of the boundary layer flow caused by a linearly extending sheet in a nanofluid was inspected by Makinde and Aziz (Makinde and Aziz, 2011). They observed that the convective heating, thermophoresis, and Brownian motion all get more intense as the local temperature rises, which causes the thermal boundary layer to thicken. The thermal conductivity performance of carbon nanotubes in fluid flow over a stretching sheet was discovered by Haq et al. (Haq et al., 2015). Sheikholeslami et al. (Sheikholeslami et al., 2016) discovered the impacts of Lorentz forces on free convective flow in the presence of nanofluid with thermal radiation. A two-dimensional time-independent flow conveying nanofluid toward a thin needle was deliberated by Soid et al. (Soid et al., 2017) where the existence of multiple solutions was reported. Bakar et al. (Bakar et al., 2018) looked into the stability analysis of mass suction impacts through a shrinking/stretching cylinder considering the nanoparticles. Kamal et al. (Kamal et al., 2019) investigated the flow of nanomaterial through a stretchable/shrinkable sheet with a chemical reaction effect. A two-dimensional magneto mixed convection flow induced by a shrinking/stretching plate in a nanofluid was investigated by Jumana et al. (Jumana et al., 2020). Johan and Mansur (Johan and Mansur, 2021) examined the features of dusty nanomaterial flow and thermal transport analysis past a stretchable sheet with a slip boundary. They used three kinds of particles, namely, alumina, copper, and titania. Shahzad et al. (Shahzad et al., 2022) scrutinized the influence of the slip effect on the flow and heat transport incorporated by copper nanofluid with different shape factors through a heated stretched sheet and found that the platelet shape factor particles have a greater rate of heat transfer compared to other shape factors. Shamshuddin et al. (Shamshuddin et al., 2024a) examined the ohmic and ferromagnetic effects on the flow of nanofluid through a porous rotating disk. They discovered that in normal fluid and nanofluid, the increased suction velocity suppresses the fluid velocity produced by the surface's porosity. Recently, Shamshuddin et al. (Shamshuddin et al., 2024b) explored the impact of electromagnetic on the radiative flow of tri-hybrid nanofluid through a bidirectional stretchy surface in penetrable media. The factors of the surface frictional force of the ternary hybrid nanofluids are found to decrease with increasing the Lorentz force and number of surface pores.

The problem of sheets stretching or shrinking in a viscous fluid has caught a lot of concentration as it has numerous applications in physics, engineering, and other scientific disciplines. It frequently occurs in practical issues that have attracted a lot of research attention because of their wide range of significance in fields like the production of glass fibre, glass blowing, metal extrusion, transportation, microfluidics, paper production, hot rolling, space, and acoustics (see Fisher (Fisher, 1976)). The BLF over an ongoing solid kind surface flowing at uniform motion was initially studied by Sakiadis (Sakiadis, 1961) in light of these applications. Numerous authors (Chen and Char, 1988; Ishak et al., 2009; Mi, 2015; Guo and Fu, 2019; Wang, 2019; Zhao et al., 2019; Zi and Wang, 2019) have thought about different elements of this problem and found similarity solutions since the groundbreaking research conducted by Crane (Crane, 1970), who provided an exact solution for the 2D steady flow caused by a stretchable surface in a quiescent fluid. Instead of focusing on the scenario of a stretched sheet, researchers instead looked at the scenario of a shrinking sheet. According to Goldstein (Goldstein, 1965), this new kind of flow of shrinking sheet is fundamentally a backward flow. The steady flow across a shrinkable sheet was studied by Miklavčič and Wang (Miklavčič and Wang, 2006). They discovered that mass suction is necessary to continue the flow across a shrinkable sheet. Waini et al. (Waini et al., 2019) examined the dependency of time-varying flow along with thermal transport across a shrinking/stretching sheet incorporated with hybrid nanofluids and provided multiple solutions.

The examination of cross-flow began following the early studies by Prandtl (Prandtl, 1946a) and Blasius (Blasius, 1908) that included the flow over a smooth surface caused by thin viscosity. Prandtl (Prandtl, 1946b) is believed to be the initial researcher to publish the findings for uniform pressure gradients flowing through a finite yawed cylinder. Weidman et al. (Weidman, 2017) examined the boundary layer via cross-flow generated by transverse plate motions. The work of Weidman was recently expanded by (Roşca et al., 2021) by taking into account rotational stagnation-point flow that transports hybrid nanofluids along a permeable shrinking or stretching surface. It was discovered that both stretching and shrinking surfaces can have multiple solutions to the fundamental similarity equations.

The phenomena of an irregular heat sink or source have applications in both engineering and medicine, involving the recovery of crude oil, the construction of thrust bearings, and the cooling of metallic sheets, etc. In the presence of an irregular heat sink/source, Tawade et al. (Tawade et al., 2016) addressed the motion of the MHD unsteady thin film and heat transfer past a stretchable sheet. It was determined that irregular heat parameters are crucial to the effectiveness of heat transfer. Thumma et al. (Thumma et al., 2017) revealed that the stretching of a sheet caused the MHD convective motion of nanofluid to have a changeable

heat sink or source. To obtain the solution, a well-known Keller-Box numerical approach is utilized. Kumar et al. (Kumar et al., 2020) looked at the movement of hybrid ferrofluids film and heat transfer in the inclusion of radiation and erratic heat source/sink (EHSE/EHSK). The rate of heat transfer is believed to be greater in hybrid ferrofluids than in ferrofluids. In addition, the velocity of the fluid and temperature tend to decline as film thickness parameters increase. Areekara et al. (Areekara et al., 2021) investigated the impact of an irregular heat source/sink on the fluid flow of nanofluid past a nonlinear stretching sheet. They observed that positive correlations exist between the radiative heat flux and the rate of heat transfer. A negative sensitivity to the rate of heat transfer is shown by the exponential heat source. Akram et al. (Akram et al., 2022) discussed the concepts of non-linear stretching and EHS/SHS to describe the heat transfer through the stretchable cylinder. It is discovered that the temperature distribution in the fluid region is being disrupted by the non-linear stretching rate and the source of heat.

The scrutiny of second law analysis or, EG (entropy generation) in fluid flow and heat transport is a prominent area of study. Energy losses resulting from chemical processes, diffusion, solid-surface friction, and the viscosity of fluids all contribute to the production of entropy in thermodynamic systems. As a result, the formation of entropy generation (EG) has drawn a lot of attention to applications including heat exchangers, turbo machinery, and electronics cooling. Aiboud and Sauoli (Aiboud and Saouli, 2010) scrutinized the entropy optimized in viscoelastic flow through a flexible surface subjected to the magnetic field. The effect of slip across a heated vertical surface in entropy-optimized flow was calculated by But et al. (Butt et al., 2012). Slips have been found to allow for the control and adjustment of entropy formation in thermal systems. Abolbashari et al. (Abolbashari et al., 2014) employed HAM to examine, EG in magneto nanofluid flow near an unsteady stretched surface with H_2O-base liquid and several nanoparticle types. Tlau and Ontela (Tlau and Ontela, 2019) examined the role of magnetohydrodynamics on nanomaterial entropy-optimized flow from an inclined channel with a heat source/sink embedded in a porous media. Entropy optimization of nanomaterials flow across two stretchable rotating disks with effects of bioconvection was examined by Khan et al. (Khan et al., 2020). Mondal et al. (Mondal et al., 2021) used trapezoidal lid-driven enclosures with, EG to study the Lorentz forces on the constant buoyant flow of Al_2O_3 nanoparticles. According to the calculations, the average Nusselt and Sherwood numbers, and aspect ratio all decrease with increasing the percentage of nanoparticle volume.

The literature that is currently accessible indicates that no exploration has been performed on the entropy generation of the radiative cross-flow stimulated with nanofluid from a porous expanding/contracting sheet with an asymmetrical heat source/sink. The present investigation fills a research gap by demonstrating cross-flow and heat transfer towards a stagnation point of nanofluid via an expanding/contracting sheet with asymmetrical heat sink/source and thermal radiation. The proposed model is originally described via a highly nonlinear system of PDEs. The PDEs are rehabilitated into ODEs by using the proper similarity variables and then solved by employing a bvp4c solver. Multiple solutions are provided for certain values of the parameters such as mass suction and shrinking sheet. The study described in this paper was driven by the following research questions.

- What impact does have on the skin friction and Nusselt number by raising the suction parameter against the stretching/shrinking parameter?
- How can the separation of the boundary layer be controlled in the presence of nanoparticles and stretching/shrinking parameters along with suction?
- What influence do Brinkman, temperature difference parameters, and TiO_2 nanoparticles have on the entropy profiles?

2 Description of the flow problem

The nanofluids' stagnation points radiative cross flow and thermal system characteristics past a contracting/expanding surface with the mutual influence of mass suction and EHSE/EHSK are taken in this study. As portrayed in Figure 1, (x_a, y_a) are Cartesian coordinates measured along the horizontal and vertical surface of the sheet, respectively, with the flow occurring in the domain $y_a \geq 0$. Nanofluid is a mixture of regular fluid (water) and single titanium dioxide (TiO_2) nanoparticles. The investigational features of the (water/TiO_2) nanomaterials are taken to be uniform. In addition, the horizontal surface of the sheet is assumed to have a variable velocity of $u_a = \varepsilon_b{}^{2/3} v_f{}^{1/3} x_a{}^{1/3} \gamma_b = u_{wa}(x_a)\gamma_b$, where γ_b refers to the expanding/contracting factor with $\gamma_b < 0$, $\gamma_b > 0$ and $\gamma_b = 0$ signify the particular cases of the shrinking, stretching, and stationary/static sheet, respectively. In the meantime, ε_b indicates the positive constant and v_f is the kinematic viscosity of the regular (water) fluid. The ambient or far-field (nanofluid) is also supposed to have a linear velocity of $u_{ex}(y_a) = \varepsilon_b y_a$, see Weidman et al. (Weidman, 2017). Moreover, the mass suction/injection or transpiration velocity at the surface of the sheet is $v_{wa}(x_a)$ with $v_{wa}(x_a) < 0$ refers to the case of injection and $v_{wa}(x_a) > 0$ refers to the case of suction while $v_{wa}(x_a) = 0$ indicating the impermeable surface of the sheet. It is also supposed that the constant temperature of the sheet is T_{wa}, while T_∞ represents the free stream temperature (inviscid fluid). With the help of these aforesaid assumptions, the governing equations in the Cartesian form are written as (Weidman, 2017; Roşca et al., 2021):

$$\frac{\partial u_a}{\partial x_a} + \frac{\partial v_a}{\partial y_a} = 0, \tag{1}$$

$$\rho_{nf}\left(u_a \frac{\partial u_a}{\partial x_a} + v_a \frac{\partial u_a}{\partial y_a}\right) = \mu_{nf} \frac{\partial^2 u_a}{\partial y_a^2}, \tag{2}$$

$$\left(\rho c_p\right)_{nf}\left(u_a \frac{\partial T_a}{\partial x_a} + v_a \frac{\partial T_a}{\partial y_a}\right) = k_{nf} \frac{\partial^2 T_a}{\partial y_a^2} - \frac{\partial Q_{rad}}{\partial y_a} + \frac{k_{nf} u_{wa}(x_a)}{x_a \nu_{nf}} \begin{bmatrix} A_b^*\left(T_{wa} - T_\infty\right)e^{-\eta} + \\ B_b^*\left(T_a - T_\infty\right) \end{bmatrix}, \tag{3}$$

with boundary conditions (BCs) are:

$$\begin{aligned} &u_a = \gamma_b u_{wa}(x_a), v_a = v_{wa}(x_a), T_a = T_{wa} \text{ at } y_a = 0, \\ &\frac{\partial u_a}{\partial y_a} \to \frac{\partial u_{ex}}{\partial y_a} = \varepsilon_b, T_a \to T_\infty \text{ as } y_a \to \infty. \end{aligned} \tag{4}$$

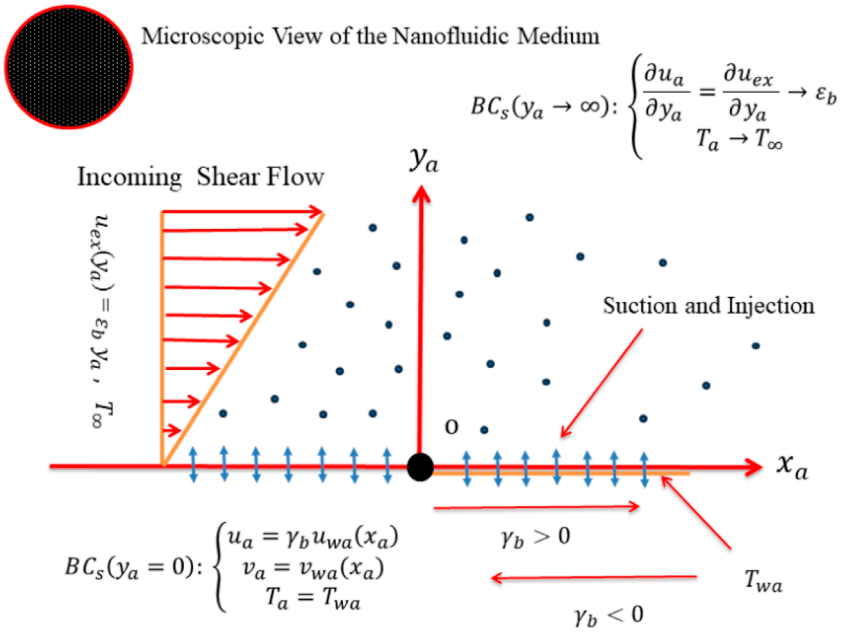

FIGURE 1
Physical model of the problem.

In Eqs 1–4, u_a and v_a are the nanofluid velocities in the corresponding x_a, and y_a directions, T_a the temperature of the nanofluid, A_b^* the exponentially decaying space coefficients, and B_b^* the temperature-dependent heat source/sink. Therefore, the heat source or absorption phenomenon is produced due to the positive value of A_b^* and B_b^* while the phenomenon of heat generation or sink is found by the negative value of both A_b^* and B_b^*.

The radiation heat flux Q_{rad} is expressed by the Rosseland approach as:

$$Q_{rad} = -\frac{4\sigma_a}{3k_a}\frac{\partial T_a^4}{\partial y_a}. \tag{5}$$

Here, the Stefan Boltzmann constant and the mean absorption coefficient are denoted by k_a and σ_a, respectively. Moreover, the term T_a^4 is simplified further by using the Taylor series at T_∞ and overlooking the power of higher-order yields:

$$T_a^4 \cong 4T_a T_\infty^3 - 3T_\infty^4. \tag{6}$$

In addition, executing Eqs 5, 6 into Eq 3 yields the final form:

$$\left(\rho c_p\right)_{nf}\left(u_a\frac{\partial T_a}{\partial x_a} + v_a\frac{\partial T_a}{\partial y_a}\right) = k_f\left(\frac{k_{nf}}{k_f} + \frac{4}{3}N_r\right)\frac{\partial^2 T_a}{\partial y_a^2} + \frac{k_{nf}u_{wa}(x_a)}{x_a v_{nf}}\begin{bmatrix} A_b^*(T_{wa} - T_\infty)e^{-\eta} + \\ B_b^*(T_a - T_\infty)\end{bmatrix}, \tag{7}$$

where $N_r = \frac{4\sigma_a T_\infty^3}{k_a k_f}$ signifies the thermal radiation parameter.

Furthermore, k_{nf} indicates the thermal conductivity of the essential posited nanofluid (NFD), $\left(\rho c_p\right)_{nf}$ indicates the heat capacitance of the NFD, ρ_{nf} indicates the density of the NFD, and μ_{nf} indicates the absolute viscosity of the NFD. The correlation of these NFDs is written as follows:

TABLE 1 The physical aspects of (TiO_2/water) nanofluid.

Physical properties	Water	TiO_2
$\rho(kg/m^3)$	997.1	4,250
$c_p(J/kgK)$	4,179	686.2
$k(W/mK)$	0.613	8.9528
Pr	6.2	-

$$\begin{cases} k_{nf} = \frac{k_{TiO_2} + 2k_f - 2\varphi_{TiO_2}\left(k_f - k_{TiO_2}\right)}{k_{TiO_2} + 2k_f + \varphi_{TiO_2}\left(k_f - k_{TiO_2}\right)}, \frac{\left(\rho c_p\right)_{nf}}{\left(\rho c_p\right)_f} = \varphi_{TiO_2}\left(\frac{\left(\rho c_p\right)_{TiO_2}}{\left(\rho c_p\right)_f}\right) + \left(1 - \varphi_{TiO_2}\right), \\ \frac{\rho_{nf}}{\rho_f} = \varphi_{TiO_2}\left(\frac{\rho_{TiO_2}}{\rho_f}\right) + \left(1 - \varphi_{TiO_2}\right), \frac{\mu_{nf}}{\mu_f} = \left(1 - \varphi_{TiO_2}\right)^{-2.5}. \end{cases} \tag{8}$$

Here, k_f, ρ_f, and μ_f refer to the thermal conductivity, the density, and the absolute viscosity of the base (water) fluid while the heat capacity at constant pressure is represented via c_p. Therefore, φ_{TiO_2} symbolizes the titania nanoparticles volume fraction and the special case $\varphi_{TiO_2} = 0$ reduces the Eqs 8 to a normal or a regular fluid (water). In addition, Table 1 displays the physical data of the titania (TiO_2) nanoparticles and the regular fluid (water).

For the considered model, the similarity transformations that can be expressed to further simplify the procedure for mathematical

analysis are as follows:

$$\eta = \left(\varepsilon_b/\upsilon_f\right)^{1/3}\frac{y_a}{x_a^{1/3}}, u_a = \varepsilon_b{}^{2/3}\upsilon_f^{1/3}x_a^{1/3}G'(\eta), H(\eta) = \frac{T_a - T_\infty}{T_{wa} - T_\infty},$$
$$v_a = -\frac{\varepsilon_b{}^{1/3}\upsilon_f^{2/3}}{3x_a^{1/3}}[2G(\eta) - \eta G'(\eta)], \tag{9}$$

which provides the opportunity to describe flows extremely broadly, regardless of the system size. Also, the prime corresponds to the derivative with respect to η, H is the non-dimensional temperature distribution, G describes the non-dimensional quantities, and G' is the dimensionless velocity profile. However, the mass suction/injection velocity at the surface of the sheet is written as:

$$v_{wa}(x_a) = -\frac{2}{3}\left(\frac{\varepsilon_b\upsilon_f^2}{x_a}\right)^{\frac{1}{3}} f_{wa}. \tag{10}$$

In Eq. 10, f_{wa} is the constant mass suction/blowing constraint with $f_{wa} = 0$, $f_{wa} < 0$ and $f_{wa} > 0$ describe the phenomena of impermeable, blowing, and suction, respectively.

With the help of similarity transformations (9), the continuity Eq 1 of the governing model is satisfied while the rest of Eqs 2, 7 equations change to the resulting known ordinary (similarity) differential equations (ODEs) as:

$$\frac{\mu_{nf}/\mu_f}{\rho_{nf}/\rho_f}G''' + \frac{2}{3}GG'' - \frac{1}{3}G'^2 = 0, \tag{11}$$

$$\left(\frac{k_{nf}}{k_f} + \frac{4}{3}N_r\right)H'' + \frac{2}{3}\Pr\frac{\left(\rho c_p\right)_{nf}}{\left(\rho c_p\right)_f}GH' + \frac{\left(\frac{k_{nf}}{k_f}\right)\left(\frac{\rho_{nf}}{\rho_f}\right)}{\left(\frac{\mu_{nf}}{\mu_f}\right)}\left(A_b^* e^{-\eta} + B_b^* H\right) = 0, \tag{12}$$

along with border conditions:

$$G(0) = f_{wa}, G'(0) = \gamma_b, H(0) = 1 \text{ at } \eta = 0,$$
$$G''(\eta) \to 1, H(\eta) \to 0 \quad \text{as } \eta \to \infty. \tag{13}$$

In addition, Eq 11 for the case of $\varphi_{TiO_2} = 0$ is the same as equation (6.1, see Weidman et al. (Weidman, 2017)) when $\alpha = 1$, but Eq 12 with some special effects has been not taken in the same reference paper. Moreover, the dimensionless model comprised the following distinct parameters, the suction/injection f_{wa}, the expanding/contracting γ_b, and the Prandtl number $\Pr = \upsilon_f/\alpha_f$.

2.1 Gradients

The two vital physical aspects, namely, heat transfer rate and shear stress of the assumed model are of practical significance to apply by scientists or engineers. They are defined as follows:

$$C_f = \frac{\mu_{nf}}{\rho_f u_{wa}^2}\left(\frac{\partial u_a}{\partial y_a}\right)\Big|_{y_a=0}, Nu_{x_a} = -\frac{x_a k_{nf}}{k_f(T_{wa} - T_\infty)}\left(-k_{nf}\left(\frac{\partial T_a}{\partial y_a}\right) + Q_{rad}\right)\Big|_{y_a=0}. \tag{14}$$

By incorporating Eq 9 into Eq 14, the following dimensionless form yields:

$$C_f\mathrm{Re}_{x_a}^{1/2} = \frac{\mu_{nf}}{\mu_f}G''(0), \mathrm{Re}_{x_a}^{-1/2}Nu_{x_a} = -\left(\frac{k_{nf}}{k_f} + \frac{4}{3}N_r\right)H'(0). \tag{15}$$

Hence, $\mathrm{Re}_{x_a} = \frac{x_a u_{wa}}{\upsilon_f}$ refers to the local Reynolds number.

3 Second law analysis

Entropy generation (E.G.,), also known as the second law analysis, is a necessary instrument for measuring energy loss and depreciation in the effectiveness of engineering and industrial systems, such as rate and transport operations. As a result, the systems expend less energy, making, E.G., analysis and comprehension crucial. Taking into account the scenario of, E.G., for the viscous Newtonian liquid with the inclusion of nanoparticles (Abolbashari et al., 2014; Tlau and Ontela, 2019).

$$EG = \frac{1}{T_\infty^2}\left(k_{nf} + \frac{16}{3}\frac{\sigma_a T_\infty^3}{k_a}\right)\left(\frac{\partial T_a}{\partial y_a}\right)^2 + \frac{\mu_{nf}}{T_\infty}\left(\frac{\partial u_a}{\partial y_a}\right)^2. \tag{16}$$

Two fundamental elements are principally responsible for the, E.G., in the contemplated cross-flow of viscous Newtonian nanofluid. The first term in the statement, which is on the right-hand side, denotes the ensuing local heat transfer, and the final term, the consequent fluid friction or viscous dissipation. The second law analysis is defined as follows in the dimensionless form:

$$NG^* = \frac{x_a^2 T_\infty^2}{k_f(T_{wa} - T_\infty)^2}EG. \tag{17}$$

The following formulas are obtained by incorporating the similarity transformations from Eq 9 into Eq 16. Hence,

$$NG^* = \left(\frac{k_{nf}}{k_f} + \frac{4}{3}N_r\right)\mathrm{Re}_{x_a}H'^2 + \frac{\mu_{nf}}{\mu_f}\mathrm{Re}_{x_a}\frac{Br_b}{\Omega_b}G'^2, \tag{18}$$

where Ω_b the dimensionless temperature difference and Br_b the Brinkman number. Consequently, they are represented mathematically as:

$$\Omega_b = \frac{(T_{wa} - T_\infty)}{T_\infty}, Br_b = \frac{\mu_f u_{wa}^2}{k_f(T_{wa} - T_\infty)}. \tag{19}$$

4 Methodology

This section demonstrates the analysis of the assumed cross-flow and the suspension of nanofluid for heat transfer. The requisite model equations are expressed as highly nonlinear ODEs (11) and (12) along with BCs (13) using similarity variables (9). A built-in function named bvp4c included in the MATLAB software is used to work out these equations numerically. It ought to be noted that the scheme of the finite difference is the foundation for the bvp4c package, which is further highlighted by the 3-stage Lobatto IIIA procedure. To instigate the bvp4c method, the transmuted ODEs are modified into a first-order system by launching new-fangled variables. By establishing this process, let

$$G = A_1, G' = A_2, G'' = A_3, H = A_4, H' = A_5. \tag{20}$$

Substituting Eq. 20 into Eqs 11, 12 along with BCs Eq. 13 we obtain the set of first-order ODEs as follows:

10.3389/fmats.2024.1391066

$$\frac{d}{d\eta}\begin{pmatrix} A_1 \\ A_2 \\ A_3 \\ A_4 \\ A_5 \end{pmatrix} = \begin{pmatrix} A_2 \\ A_3 \\ \frac{(\rho_{nf}/\rho_f)}{(\mu_{nf}/\mu_f)}\left[\frac{1}{3}A_2^2 - \frac{2}{3}A_1A_3\right] \\ A_5 \\ \frac{1}{\left(\frac{k_{nf}}{k_f} + \frac{4}{3}N_r\right)}\left[-\frac{2}{3}\Pr\frac{(\rho c_p)_{nf}}{(\rho c_p)_f}A_4A_2 - \frac{(k_{nf}/k_f)(\rho_{nf}/\rho_f)}{(\mu_{nf}/\mu_f)}\left(A_b^* e^{-\eta} + B_b^* A_4\right)\right] \end{pmatrix}, \quad (21)$$

with BCs

$$A_1(0) = f_{wa}, A_2(0) = \gamma_b, A_4(0) = 1, A_3(\infty) = 1, A_4(\infty) = 0. \quad (22)$$

The code desired initial estimations at the posited mesh point to solve Eq 21 and the corresponding conditions Eq. 22. The polynomial used in the collective type yields a continuous result. A fourth order accuracy set that is equally distributed over the spatial intervals where the function is integrated provides the result. The limitation at a distance $(\eta \to \infty)$ is replaced by the value $(\eta = \eta_\infty = 8)$ in many successful boundary layer theory applications, and the relative tolerance error is pre-defined as 10^{-6}. Additionally, the residual of the smooth output serves as the basis for both the mesh selection and error control. The initial mesh comprises four identical discredited points on the range $(0, \eta_\infty = 8)$, and the mesh selection is then automatically changed using the bvp4c package. The problem now has two possible solutions, which means that the bvp4c package needed two alternative guesses for the unstable and stable solutions. The early initial presumes for the upper solution is moderately straightforward, whilst selecting a guess for the second solution is fairly challenging. Merkin et al. (Merkin, 1986) and Weidman et al. (Weidman et al., 2006) claim that the upper solution is physically stable and reliable but the lower solution is unstable and not physically dependable since the outcome only exists for a specific range of shrinking sheets.

4.1 Validation of the MATLAB bvp4c solver

This subsection of the work specifies the rationality or validity, accuracy, and correctness of the considered MATLAB bvp4c solver for the special limiting case. To confirm this rationality, the friction factor outcomes for both branches (stable and unstable) results owing to several values of the shrinking constraint with prior research work when f_{wa}, and φ_{TiO_2} are equal to zero. Therefore, Table 2 displays the results as well as a comparison to those of previous research work/literature. Thus, we can conclude that our results are trustworthy because our data closely aligns with those that have already been published.

TABLE 2 Numerical comparison of outcomes for friction factor owing to several values of the shrinking parameter when $f_{wa} = 0$, and $\varphi_{TiO_2} = 0$.

$\gamma_b < 0$	Waini et al. (Waini et al., 2020)		Present	
	Stable	Unstable	Stable	Unstable
0.1	0.993440	−0.017703	0.993440	−0.017703
0.2	0.971925	−0.018388	0.971925	−0.018388
0.3	0.931424	−0.000045	0.931424	−0.000045
0.4	0.864452	0.044824	0.864452	0.044824
0.5	0.752585	0.134657	0.752585	0.134657

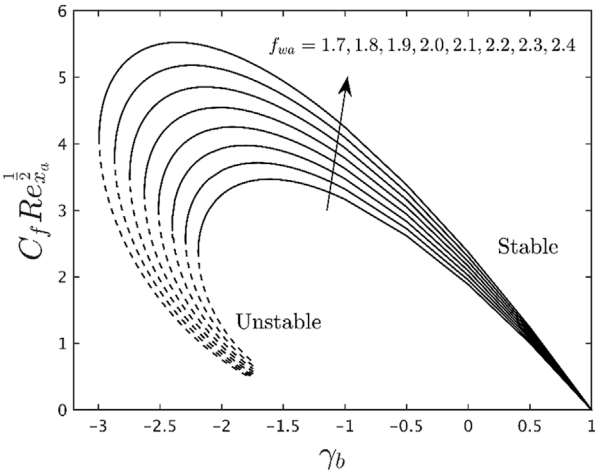

FIGURE 2
Impact of f_{wa} on $C_f \mathrm{Re}_{x_a}^{1/2}$ *versus* γ_b.

5 Analysis of the results

The current portion of the work describes the binary (stable and unstable) solutions for a certain region or area of the dimensionless mass suction parameter as well as the contracting parameter γ_b due to the variations in one physical parameter at the time of computations while the other factors are taken to be fixed. To ease analysis, the values of the basic physical influential parameters are $\varphi_{TiO_2} = 0.025$, $\gamma_b = -2.0$, $f_{wa} = 1.5$, $A_b^* = 0.1$, $N_r = 0.05$, and $B_b^* = 0.1$. Table 1 reveals the experimental data of titania (TiO_2) nanoparticles. Meanwhile, the comparison of the upshots for the unusual case is demonstrated in Table 2. Besides, the outcomes of the friction factor, heat transfer, and entropy generation are captured in various graphs (see Figures 2–8) of the nanofluid for the unstable and stable branches owed to the influence of the several comprised factors while their quantitative outputs are shown in Tables 3, 4. However, the branches of stable solutions (SBES), as well as solutions of unstable (USBES) are categorized by the black solid and black dash lines, respectively. The position in the graph or picture where both (SBES and USBES) curves meet at a single point is called the bifurcation or critical point. In this study, the SBES and USBES are invented only for the case of shrinking parameters.

The numerical data of the gradients (skin friction and heat transfer rate) with the impression of the several distinguished factors corresponding to water-based Titania nanofluid are illustrated in Tables 3, 4 for the SBSE and USBES, respectively. Upshots divulge that the friction factor upsurges for the SBSE owed to the superior values of φ_{TiO_2} and f_{wa} while the branch of USBES behaves distinctly with variations in the mass suction parameter f_{wa} but similarly with higher impacts of φ_{TiO_2}. Notably, the shear stress of the nanofluid is

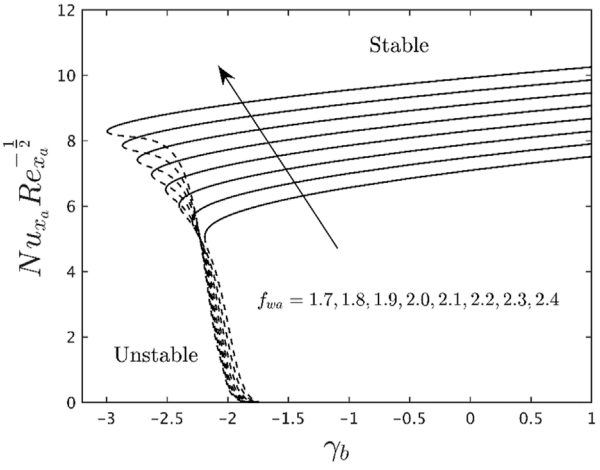

FIGURE 3
Impact of f_{wa} on $Nu_{x_a}\mathrm{Re}_{x_a}^{-1/2}$ *versus* γ_b.

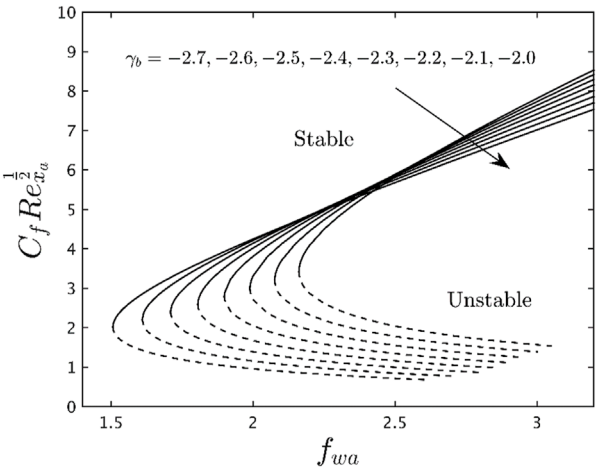

FIGURE 4
Impact of γ_b on $C_f\mathrm{Re}_{x_a}^{1/2}$ *versus* f_{wa}.

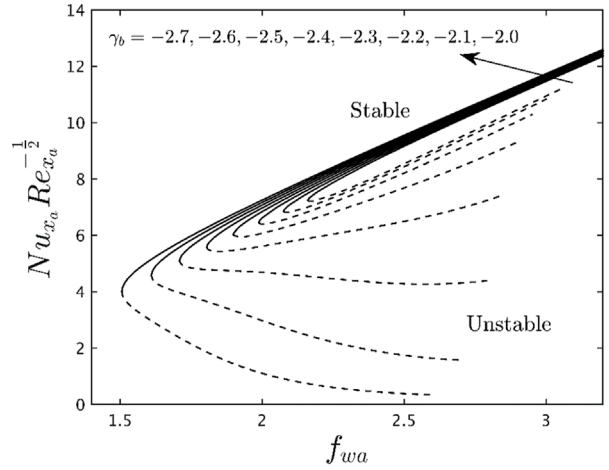

FIGURE 5
Impact of γ_b on $Nu_{x_a}\mathrm{Re}_{x_a}^{-1/2}$ *versus* f_{wa}.

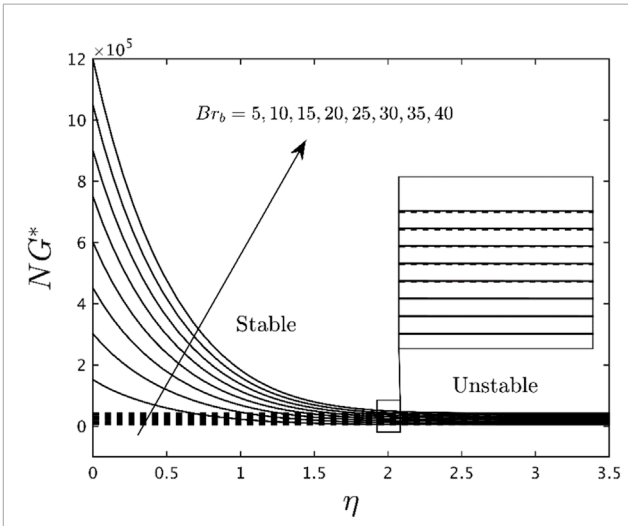

FIGURE 6
Impact of Br_b on NG^* *versus* η.

highest and lowest for the SBES and USBES with mass suction f_{wa}. In contrast, the heat transfer escalates for both (SBES and USBES) results with superior consequences of φ_{TiO_2}. Therefore, owing to the rise in the heat source parameter $A_b^*, B_b^* > 0$, the heat transfer shrinkages in the SBES as well as the USBES are endlessly enriching due to the higher role of the heat sink parameter $A_b^*, B_b^* < 0$. In addition, the lowest and highest heat transfer approximations are perceived for the branch of SBES and USBES with the following selected values $A_b^*, B_b^* = 0.9$, and $\varphi_{TiO_2} = 0.035$.

Figures 2, 3 show the impact of f_{wa} on the shear stress and heat transfer corresponding to (TiO_2/water) nanofluid for the SBES as well as the USBES, respectively. In this study, the dual (SBES and USBES) outcomes are possible to occur for a certain domain of the specific set of physical parameters. Therefore, the non-unique outcomes in either pictures or graphs exist for a posited shrinkable sheet. Moreover, it is clear from the above graphs that the position where both solution curves meet is at a point called the critical point. Mathematically, this point is expressed by the symbol $\gamma_b C$, where the solutions are unique $\gamma_b = \gamma_b C$. The non-unique solutions (dual) and no solutions are possible to exist for the range $\gamma_b C < \gamma_b < \infty$ and $-\infty < \gamma_b < \gamma_b C$, respectively. Besides, the outcomes refer to the shear stress and heat transfer escalating for the SBES due to the larger impact of f_{wa} while they are declined for the USBES. Physically, the motion of the nanofluid stops due to the inspiration of f_{wa} shifting the particles of the liquid moving toward the surface of the sheet and sticking with it. Hence, the friction and motion/velocity of the nanofluid hold the inverse relations, as a result, the shear stress is enhanced. Furthermore, the next eight distinct critical values −2.1903, −2.2941, −2.4016, −2.5125, −2.6274, −2.7463, −2.8686, and −2.9951 are obtained for the respective change value of f_{wa}. With the rise of f_{wa} causes an increment in the absolute value of $|\gamma_b C|$. This behavior corresponds to the superior inclusion of f_{wa} decelerating the boundary layer separation.

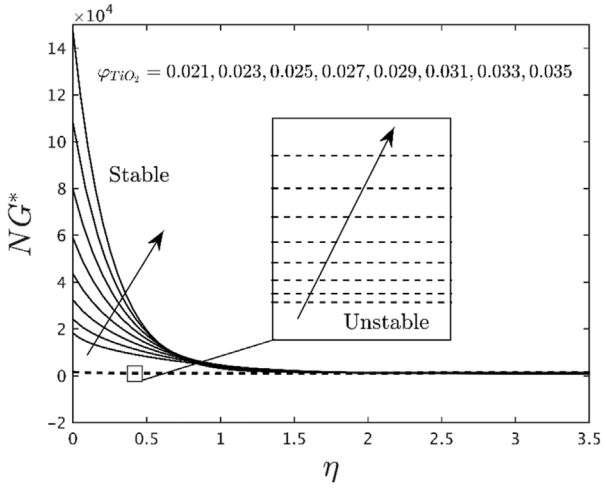

FIGURE 7
Impact of φ_{TiO_2} on NG^* *versus* η.

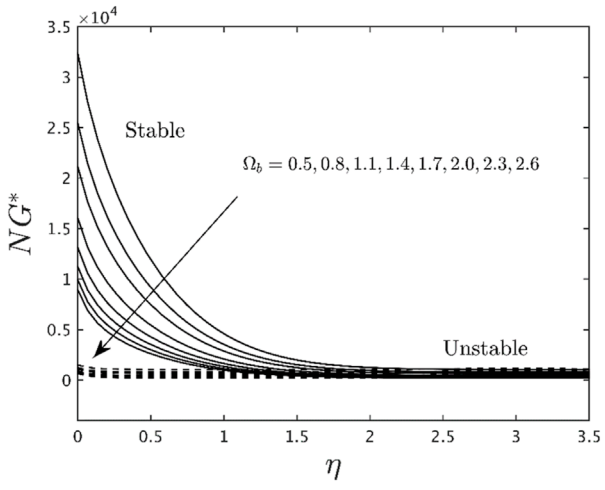

FIGURE 8
Impact of Ω_b on NG^* *versus* η.

TABLE 3 Numerical outcomes are made for the shear stress with φ_{TiO_2} and f_{wa} when $\gamma_b = -2.0$, $N_r = 0.05$, $A_b^* = 0.1$, and $B_b^* = 0.1$.

φ_{TiO_2}	f_{wa}	Shear stress	
		Stable	Unstable
0.025	1.5	5.6460767	1.0653406
0.030	-	5.8683445	1.0791223
0.035	-	6.0989946	1.0931549
0.025	1.5	5.6460767	1.0653406
0.030	2.0	8.1019827	0.7430102
0.035	2.5	10.531567	0.5628759

TABLE 4 Numerical outcomes are made for the heat transfer with φ_{TiO_2} and A_b^*, B_b^* when $\gamma_b = -2.0$, $N_r = 0.05$, and $f_{wa} = 1.5$.

φ_{TiO_2}	A_b^*, B_b^*	Heat transfer	
		Stable	Unstable
0.025	0.5	4.6336867	15.001956
0.030	-	4.6360107	15.273743
0.035	-	4.6387796	15.562330
0.025	0.5	4.6336867	15.001956
-	0.7	4.3834284	10.021935
-	0.9	4.1226401	8.2234605
0.025	−0.5	5.7491768	4.6342404
-	−0.7	5.9488839	5.2367610
-	−0.9	6.1418652	5.6895740

The impressions of γ_b on $C_f \mathrm{Re}_{x_a}^{1/2}$ and $Nu_{x_a} \mathrm{Re}_{x_a}^{-1/2}$ *versus* f_{wa} of (TiO_2/water) nanofluid for both (SBES and USBES) results are typified in Figures 4, 5, respectively. The dual (SBES and USBES) results are shown in both graphs for the case of f_{wa} due to the variations in the shrinking parameter. In both graphs, it is seen that the SBES and USBES curves congregate at a point called the critical point which is denoted by $f_{wa}C$. Meanwhile, the outcomes are unique for the case when $f_{wa} = f_{wa}C$, but the phenomena $f_{wa}C < f_{wa} < \infty$, and $-\infty < f_{wa} < f_{wa}C$ indicate the non-unique and no solutions, respectively. Besides, the shear stress decays and rises for the SBES due to the higher values of γ_b while it shrinks for the USBES. Alternatively, with the increase of γ_b, the thermal transport phenomenon uplifts for the SBES and declines for the USBES. More significantly, it is understood from the diagrams that bifurcation values like 2.1615, 2.0760, 1.9888, 1.8986, 1.8057, 1.7096, 1.6098, and 1.5066 are found due to the several values of γ_b. Also, it is noted here that the magnitude of the critical values $|f_{wa}C|$ is weakened once the shrinking parameter is boosted. This further specifies that the growth in the impacts of γ_b hastens the boundary layer (BL) separations.

With the assistance or support of entropy generation or second law analysis (SLA), the thermodynamic system performance of water-based Titania nanoparticles can be improved. Figures 6–8 describe the consequence of parameters Br_b, φ_{TiO_2}, and Ω_b on SLA (second law analysis) corresponding to the posited nanofluid for the SBES and USBES, respectively. As premeditated in Figures 6, 7, an improvement in both parameters of Br_b and φ_{TiO_2} results in an improvement of SLA for the branch of stable as well as unstable solutions. The second law analysis is also more susceptible to changes in this parameter Br_b value at the place close to the wall surface of the sheet. As increases η, susceptibility rapidly decreases. Therefore, the physical data and prior research findings are compatible with this occurrence. Conversely, Figure 8 is designed to inspect the parameter Ω_b on second law analysis of the (TiO_2/water) nanofluid for both (SBES and USBES). In general, the lower temperature

difference between the wall and its surroundings is generally caused by larger values of Ω_b, which reduces second law analysis or, EG. The aforementioned discussion leads to the conclusion that by altering the related parameters, the system's second law analysis value can be decreased to increase the solar radiation utilization system's effectiveness.

6 Conclusion

The theoretical inspection on radiative cross flow and heat transfer incorporated water-based TiO_2 nanofluid through a permeable stretching/shrinking sheet with irregular heat source/sink have been explored. The entropy generation was used to analyze the heat transfer process after the development of a computational model. Combined impacts of pertaining governing parameters like suction, expanding/contracting parameter, irregular heat source/sink parameter, radiation parameter, and volume fraction of the nanoparticles on shear stress and the heat transfer have been analyzed. The important conclusions of our research can be summed up as follows.

- The results suggest that the shear stress enhances due to f_{wa} and φ_{TiO_2}, whilst the heat transfer accelerates due to φ_{TiO_2}.
- The heat transfer rate accelerates due to the heat source $\left(A_b^*, B_b^* > 0\right)$ and decelerates due to heat sink $\left(A_b^*, B_b^* < 0\right)$.
- The entropy generation increases in the presence of Brinkman number and nanoparticle volume fraction in both solutions, while decreasing due to the higher impacts of the difference of temperature parameter in both solutions.

7 Future work

Further, this problem can also be studied by incorporating unsteady flow or mixed convection flow in addition to incorporating various physical elements such as the slip effect, chemical reaction viscous dissipation, etc. Also, this model can be extended to any non-Newtonian models of the problem along with several other impacts like shape factors of the nanoparticles, waste discharge concentration, and thermophoresis particle deposition effects.

Data availability statement

The raw data supporting the conclusions of this article will be made available by the authors, without undue reservation.

Author contributions

SE: Writing–review and editing, Writing–original draft, Validation, Software, Project administration, Investigation, Funding acquisition, Formal Analysis. UK: Writing–review and editing, Visualization, Software, Methodology, Investigation, Conceptualization. AZ: Writing–original draft, Validation, Methodology, Data curation, Conceptualization. AI: Writing–review and editing, Validation, Supervision, Investigation, Formal Analysis. NA: Writing–review and editing, Writing–original draft, Validation, Resources, Funding acquisition. HA: Writing–original draft, Visualization, Validation, Resources, Funding acquisition.

Funding

The author(s) declare that financial support was received for the research, authorship, and/or publication of this article. This work was funded by the Deanship of Scientific Research at Princess Nourah bint Abdulrahman University, through the Research Groups Program Grant no. (RGP-1444-0060).

Acknowledgments

This work was funded by the Deanship of Scientific Research at Princess Nourah bint Abdulrahman University, through the Research Groups Program Grant no. (RGP-1444-0060).

Conflict of interest

The authors declare that the research was conducted in the absence of any commercial or financial relationships that could be construed as a potential conflict of interest.

Publisher's note

References

Abolbashari, M. H., Freidoonimehr, N., Nazari, F., and Rashidi, M. M. (2014). Entropy analysis foran unsteady MHD flow past a stretching permeable surface in nanofluid. *Powder Technol.* 267, 256–267. doi:10.1016/j.powtec.2014.07.028

Aiboud, S., and Saouli, S. (2010). Entropy analysis for viscoelastic magneto-hydrodynamic flow over a stretching surface. *Int. J. Nonlinear Mech.* 45, 482–489. doi:10.1016/j.ijnonlinmec.2010.01.007

Akram, M., Jamshed, W., Goud, B. S., Pasha, A. A., Sajid, T., Rahman, M. M., et al. (2022). Irregular heat source impact on carreau nanofluid flowing via exponential expanding cylinder: a thermal case study. *Eng* 36, 102171. doi:10.1016/j.csite.2022.102171

Areekara, S., Mackolil, J., Mahanthesh, B., Mathew, A., and Rana, P. (2021). A study on nanoliquid flow with irregular heat source and realistic boundary conditions: a modified Buongiorno model for biomedical applications. *Z. für Angew. Math. Mech.* 102 (3), e202100167. doi:10.1002/zamm.202100167

Bakar, N. A. A., Bachok, N., Arifin, N. M., and Pop, I. (2018). Stability analysis on the flow and heat transfer of nanofluid past a stretching/shrinking cylinder with suction effect. *Res. Phys.* 9, 1335–1344. doi:10.1016/j.rinp.2018.04.056

Blasius, H. (1908). Grenzschichten in Flüssigkeiten mit kleiner Reibung. *Z. Math. Phys.* 56, 1–37.

Butt, A. S., Munawar, S., Ali, A., and Mehmood, A. (2012). Entropy generation in hydrodynamic slip flow over a vertical plate with convective boundary. *J. Mech. Sci. Technol.* 26, 2977–2984. doi:10.1007/s12206-012-0701-3

Chen, C. K., and Char, M. I. (1988). Heat transfer of a continuous, stretching surface with suction or blowing. *J. Math. Anal. Appl.* 135, 568–580. doi:10.1016/0022-247x(88)90172-2

Choi, S. U., and Eastman, J. A. (1995). *Enhancing thermal conductivity of fluids with nanoparticles (No. ANL/MSD/CP-84938; CONF-951135-29)*. IL (United States): Argonne National Lab.

Crane, L. J. (1970). Flow past a stretching plate. *Z. Angew. Math. Phys.* 21, 645–647. doi:10.1007/bf01587695

Eastman, J. A., Choi, S. U. S., Li, S., Yu, W., and Thompson, L. J. (2001). Anomalously increased effective thermal conductivities of ethylene glycol-based nanofluids containing copper nanoparticles. *Appl. Phys. Lett.* 78 (6), 718–720. doi:10.1063/1.1341218

Fisher, E. G. (1976). *Extrusion of plastics*. New York, NY: Wiley.

Goldstein, S. (1965). On backward boundary layers and flow in converging passages. *J. Fluid Mech.* 21, 33–45. doi:10.1017/s0022112065000034

Guo, X., and Fu, Z. (2019). An initial and boundary value problem of fractional Jeffreys' fluid in a porous half space. *Comput. Math. Comp.* 78 (6), 1801–1810. doi:10.1016/j.camwa.2015.11.020

Haq, R. U., Nadeem, S., Khan, Z. H., and Noor, N. F. M. (2015). Convective heat transfer in MHD slip flow over a stretching surface in the presence of carbon nanotubes. *Phys. B Condens. Matter* 457, 40–47. doi:10.1016/j.physb.2014.09.031

Ishak, A., Nazar, R., and Pop, I. (2009). Boundary layer flow and heat transfer over an unsteady stretching vertical surface. *Meccanica* 44, 369–375. doi:10.1007/s11012-008-9176-9

Johan, N. A., and Mansur, S. (2021). Boundary layer flow of dusty nanofluid over stretching sheet with partial slip effects. *J. Advan. Res. Fluid Mech. Therm. Sci.* 87 (2), 118–126. doi:10.37934/arfmts.87.2.118126

Jumana, S. A., Murtaza, M. G., Ferdows, M., Makinde, O. D., and Zaimi, K. (2020). Dual solutions analysis of melting phenomenon with mixed convection in a nanofluid flow and heat transfer past a permeable stretching/shrinking sheet. *J. Nanofluids* 9 (4), 313–320. doi:10.1166/jon.2020.1761

Kamal, F., Zaimi, K., Ishak, A., and Pop, I. (2019). Stability analysis of MHD stagnation-point flow towards a permeable stretching/shrinking sheet in a nanofluid with chemical reactions effect. *Sains Malay* 48 (1), 243–250. doi:10.17576/jsm-2019-4801-28

Khan, N. S., Shah, Q., Bhaumik, A., Kumam, P., Thounthong, P., and Amiri, I. (2020). Entropy generation in bioconvection nanofluid flow between two stretchable rotating disks. *Sci. Rep.* 10, 4448. doi:10.1038/s41598-020-61172-2

Khan, W. A., and Pop, I. (2010). Boundary-layer flow of a nanofluid past a stretching sheet. *Int. J. Heat. Mass Transf.* 53 (11-12), 2477–2483. doi:10.1016/j.ijheatmasstransfer.2010.01.032

Kumar, K. A., Sandeep, N., Sugunamma, V., and Animasaun, I. L. (2020). Effect of irregular heat source/sink on the radiative thin film flow of MHD hybrid ferrofluid. *J. Therm. Anal. Calorim.* 139, 2145–2153. doi:10.1007/s10973-019-08628-4

Makinde, O. D., and Aziz, A. (2011). Boundary layer flow of a nanofluid past a stretching sheet with a convective boundary condition. *Int. J. Therm. Sci.* 50 (7), 1326–1332. doi:10.1016/j.ijthermalsci.2011.02.019

Merkin, J. H. (1986). On dual solutions occurring in mixed convection in a porous medium. *J. Eng. Math.* 20, 171–179. doi:10.1007/bf00042775

Mi, L. (2015). Boundary behavior for the solutions to Dirichlet problems involving the infinity-Laplacian. *J. Math. Anal. Appl.* 425 (2), 1061–1070. doi:10.1016/j.jmaa.2014.12.070

Miklavčič, M., and Wang, C. Y. (2006). Viscous flow due to a shrinking sheet. *Q. Appl. Math.* 64, 283–290. doi:10.1090/s0033-569x-06-01002-5

Mondal, P., Mahapatra, T. R., and Parveen, R. (2021). Entropy generation in nanofluid flow due to double diffusive MHD mixed convection. *Heliyon* 7, e06143. doi:10.1016/j.heliyon.2021.e06143

Prandtl, L. (1946a). *Über Flüssigkeitsbewegung bei sehr kleiner Reibung, Verh. III. Int. Math. Kongr. Heidelberg*. Leipzig: Teubner, 484–491.

Prandtl, L. (1946b). On boundary layers in three-dimensional flow. *Rep. Aero. Res. Coun. Lond. No.* 9829.

Roşca, N. C., Roşca, A. V., Jafarimoghaddam, A., and Pop, I. (2021). Cross flow and heat transfer past a permeable stretching/shrinking sheet in a hybrid nanofluid. *Int. J. Numer. Meth. Heat. Fluid Flow.* 31, 1295–1319. doi:10.1108/hff-05-2020-0298

Sakiadis, B. C. (1961). Boundary-layer behavior on continuous solid surfaces: I. Boundary-layer equations for two-dimensional and axisymmetric flow. *Am. Inst. Chem. Eng. J.* 7, 26–28. doi:10.1002/aic.690070108

Shahzad, A., Liaqat, F., Ellahi, Z., Sohail, M., Ayub, M., and Ali, M. R. (2022). Thin film flow and heat transfer of Cu-nanofluids with slip and convective boundary condition over a stretching sheet. *Sci. Rep.* 12, 14254. doi:10.1038/s41598-022-18049-3

Shamshuddin, M. D., Panda, S., Pattnaik, P. K., and Mishra, S. R. (2024a). Ferromagnetic and ohmic effects on nanofluid flow via permeability rotative disk: significant interparticle radial and nanoparticle radius. *Phys. Scr.* 99, 055206. doi:10.1088/1402-4896/ad35f8

Shamshuddin, M. D., Salawu, S. O., Panda, S., Mishra, S. R., Alanazy, A., and Eid, M. R. (2024b). Thermal case exploration of electromagnetic radiative tri-hybrid nanofluid flow in Bi-directional stretching device in absorbent medium: SQLM analysis. *Case Stud. Therm. Eng.* 60, 104734. doi:10.1016/j.csite.2024.104734

Sheikholeslami, M., Hayat, T., and Alsaedi, A. (2016). MHD free convection of Al_2O_3-water nanofluid considering thermal radiation: a numerical study. *Int. J. Heat. Mass Transf.* 96, 513–524. doi:10.1016/j.ijheatmasstransfer.2016.01.059

Soid, S. K., Ishak, A., and Pop, I. (2017). Boundary layer flow past a continuously moving thin needle in a nanofluid. *Appl. Therm. Eng.* 114, 58–64. doi:10.1016/j.applthermaleng.2016.11.165

Tawade, J., Abel, M. S., Metri, P. G., and Koti, A. (2016). Thin film flow and heat transfer over an unsteady stretching sheet with thermal radiation, internal heating in the presence of external magnetic field. *Int. J. Adv. Appl. Math. Mech.* 3, 29–40.

Thumma, T., Beg, O. A., and Kadir, A. (2017). Numerical study of heat source/sink effects on dissipative magnetic nanofluid flow from a non-linear inclined stretching/shrinking sheet. *J. Mol. Liq.* 232, 159–173. doi:10.1016/j.molliq.2017.02.032

Tlau, L., and Ontela, S. (2019). Entropy generation in MHD nanofluid flow with heat source/sink. *SN Appl. Sci.* 1, 1672. doi:10.1007/s42452-019-1733-4

Waini, I., Ishak, A., and Pop, I. (2019). Unsteady flow and heat transfer past a stretching/shrinking sheet in a hybrid nanofluid. *Int. J. Heat. Mass Transf.* 136, 288–297. doi:10.1016/j.ijheatmasstransfer.2019.02.101

Waini, I., Ishak, A., and Pop, I. (2020). Transpiration effects on hybrid nanofluid flow and heat transfer over a stretching/shrinking sheet with uniform shear flow. *Alex. Eng. J.* 59, 91–99. doi:10.1016/j.aej.2019.12.010

Wang, Y. (2019). Multiple positive solutions for mixed fractional differential system with p-Laplacian operators. *Value Probl.* 2019, 144. doi:10.1186/s13661-019-1257-2

Weidman, P. (2017). Further solutions for laminar boundary layers with cross flows driven by boundary motion. *Acta Mech.* 228, 1979–1991. doi:10.1007/s00707-017-1810-y

Weidman, P. D., Kubitschek, D. G., and Davis, A. M. J. (2006). The effect of transpiration on self-similar boundary layer flow over moving surfaces. *Int. J. Eng. Sci.* 44, 730–737. doi:10.1016/j.ijengsci.2006.04.005

Zhao, Y., Sun, Y., Liu, Z., and Bai, Z. (2019). Basic theory of differential equations with mixed perturbations of the second type on time scales. *Adv. Differ. Equ.* 2019, 268. doi:10.1186/s13662-019-2212-3

Zi, Y., and Wang, Y. (2019). Positive solutions for Caputo fractional differential system with coupled boundary conditions. *Adv. Differ. Equ.* 2019, 80. doi:10.1186/s13662-019-2016-5

10.3389/fmats.2024.1391066

Nomenclature

A_b^*	Exponentially decaying space coefficients
C_f	Skin friction
Nu_{x_a}	Local Nusselt number
B_b^*	Temperature-dependent heat source/sink
Br_b	Brinkman number
N_r	Thermal radiation parameter
Q_{rad}	Radiation heat flux
c_p	Specific heat at constant pressure (J kg^{-1} K^{-1})
$A_b^*, B_b^* > 0$	Heat source parameter
$A_b^*, B_b^* < 0$	Heat sink parameter
f_{wa}	Suction parameter
G'	Dimensionless velocity
T_a	Temperature of the nanofluid (K)
T_{wa}	Constant temperature (K)
H	Dimensionless temperature
Pr	Prandtl number
Re_{x_a}	Local Reynolds number
T_∞	Free stream temperature (K)
$v_{wa}(x_a)$	Mass suction/injection or transpiration velocity at the surface of the sheet u_a, v_a Velocities in the x_a–, and y_a–directions, respectively (m/s)
$u_{wa}(x_a)$	Variable velocity at the surface of the sheet (m/s)
x_a, y_a	Cartesian coordinates (m)
ε_b	Positive constant
μ	Absolute viscosity (Pa s)
γ_b	Expanding/contracting factor
σ_a	Mean absorption coefficient (m^{-1})
υ	Kinematic viscosity (m^2/s)
φ	Nanoparticle volume fraction
Ω_b	Dimensionless temperature difference
k	Thermal conductivity (W/mK)
ρ	Density (kg/m^3)
η	Pseudo-similarity variable
BCs	Boundary conditions
Bvp4c	Boundary value problem of fourth-order
TiO_2	Titania nanoparticles
EG	Entropy generation
NFD	Nanofluid
PDEs	Partial differential equations
2D	Two-dimensional flow
ODEs	Ordinary differential equations
SBES	Stable branch solutions
USBES	Unstable branch solutions
nf	Nanofluid
f	Regular fluid
w	Wall boundary condition
∞	Far-field condition
$'$	Derivative w.r.t. η